A Unique Mdm2-Binding Mode of the 3-Pyrrolin-2-one- and 2-Furanone-Based Antagonists of the p53-Mdm2 Interaction

Surmiak, Ewa; Twarda-Clapa, Aleksandra; Zak, Krzysztof M.; Musielak, Bogdan; Tomala, Marcin D.; Kubica, Katarzyna; Grudnik, Przemyslaw; Madej, Mariusz; Jablonski, Mateusz; Potempa, Jan

Published in:
ACS chemical biology

DOI:
10.1021/acschembio.6b00596

ACS chemical biology

Articles

pubs.acs.org/acschemicalbiology

A Unique Mdm2-Binding Mode of the 3-Pyrrolin-2-one- and 2-Furanone-Based Antagonists of the p53-Mdm2 Interaction

Ewa Surmiak,[†,⊥] Aleksandra Twarda-Clapa,[‡,§,⊥] Krzysztof M. Zak,[‡,§] Bogdan Musielak,[†] Marcin D. Tomala,[†] Katarzyna Kubica,[†] Przemyslaw Grudnik,[‡] Mariusz Madej,[‡,§] Mateusz Jablonski,[†] Jan Potempa,[‡,§] Justyna Kalinowska-Tluscik,[†] Alexander Dömling,[∥] Grzegorz Dubin,[*,‡,§] and Tad A. Holak[*,†,§]

[†]Faculty of Chemistry, Jagiellonian University, Ingardena 3, 30-060 Krakow, Poland

[‡]Faculty of Biochemistry, Biophysics and Biotechnology, Jagiellonian University, Gronostajowa 7, 30-387 Krakow, Poland

[§]Malopolska Centre of Biotechnology, Jagiellonian University, Gronostajowa 7a, 30-387 Krakow, Poland

[∥]Faculty of Mathematics and Natural Sciences, Department of Pharmacy, University of Groningen, 9713AV Groningen, The Netherlands

Supporting Information

ABSTRACT: The p53 pathway is inactivated in almost all types of cancer by mutations in the p53 encoding gene or overexpression of the p53 negative regulators, Mdm2 and/or Mdmx. Restoration of the p53 function by inhibition of the p53-Mdm2/Mdmx interaction opens up a prospect for a nongenotoxic anticancer therapy. Here, we present the syntheses, activities, and crystal structures of two novel classes of Mdm2-p53 inhibitors that are based on the 3-pyrrolin-2-one and 2-furanone scaffolds. The structures of the complexes formed by these inhibitors and Mdm2 reveal the dimeric protein molecular organization that has not been observed in the small-molecule/Mdm2 complexes described until now. In particular, the 6-chloroindole group does not occupy the usual Trp-23 pocket of Mdm2 but instead is engaged in dimerization. This entirely unique binding mode of the compounds opens new possibilities for optimization of the Mdm2−p53 interaction inhibitors.

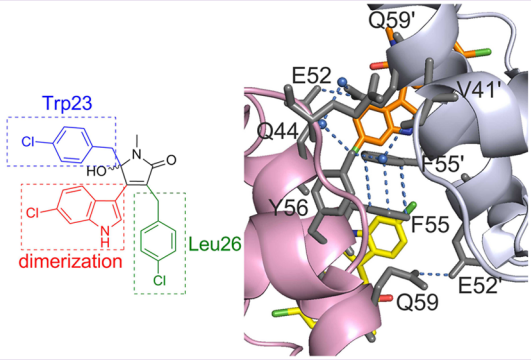

The tumor suppressor p53 protein pathway is inactivated in the majority of human cancer either by mutations within the p53 gene or by overexpression of negative regulators of p53, predominantly Mdm2 and/or Mdmx proteins. Restoration of active p53 has been demonstrated to be a promising strategy against cancer.[1−3] Mutations in the p53 encoding gene are found in about 50% of all human cancers.[1−6] In the tumors that contain the wildtype p53, liberation of its activity by disrupting the interaction with the Mdm2/Mdmx, using low-molecular-weight inhibitors, should provide an efficient, nongenotoxic anticancer therapy.[1] Although tremendous progress was observed in the latter strategy[4−6] since the initial demonstration of the efficacy of an early inhibitor nutlin-3a,[7] constant development of yet novel compounds with better pharmacological properties is sought.[8−12]

The interaction of the transactivation domain of p53 with the N-terminal domain of Mdm2 is mediated primarily by the side chains of Phe19, Trp23, and Leu26 of p53, which occupy three hydrophobic subpockets within Mdm2.[13,14] These interactions define a three finger pharmacophore which characterizes the vast majority of the currently available small-molecule Mdm2 inhibitors.[8,9] Since the early discovery by García-Echeverría *et al.* that substitution of the indole moiety of Trp23 in the p53 peptide with that of 6-chloroindole significantly potentiates Mdm2 affinity,[15] a large number of small-molecule inhibitors have been developed in which a major interaction with Mdm2 is provided by a 6-chloroindole moiety occupying the Trp23 subpocket.[16−18] Nevertheless, certain new approaches were recently proposed.[5,6,19−23]

In this study, we describe novel Mdm2 inhibitors based on the 3-pyrrolin-2-one and 2-furanone scaffolds, which by design contain the 6-chloroindole structure anchoring pharmacophore and a maximal number of halogenated phenyl groups. Crystals of the complexes formed by these inhibitors and Mdm2 unexpectedly revealed dimeric protein arrangement formed by the chloroindole−protein and protein−protein interactions in which the 6-chloroindole group does not occupy the usual Trp-23 pocket of Mdm2.

Received: July 12, 2016
Accepted: October 6, 2016
Published: October 6, 2016

DOI: 10.1021/acschembio.6b00596
ACS Chem. Biol. 2016, 11, 3310−3318

Table 1. Structures and Activity of Mdm2 Inhibitors Reported in This Study

No	Formula	K_d by NMR [μM][a]	K_d by MST [μM]	No	Formula	K_d by NMR [μM][a]	K_d by MST [μM]
1a	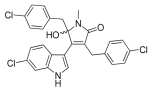	<1	0.5±0.3	**1b**	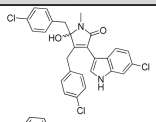	56	not active
1c	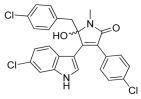	51	18.7±0.2	**1d**	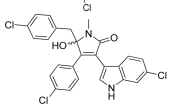	192	27.7±0.2
1e	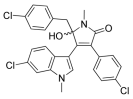	365	40.5±0.3	**1f**	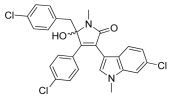	246	30.4±0.2
1g	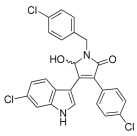	164	24.4±0.1	**1h**	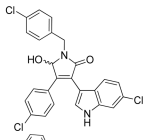	40	2.1±0.1
2a	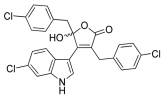	<1	3.1±04	**2b**	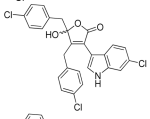	86	1.5±0.4
2c	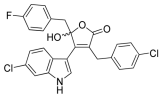	18	28.7±1.0	**2d**	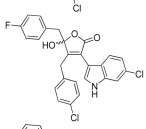	no data[b]	26.0±1.0
2e	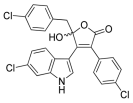	60	1.3±0.2	**2f**	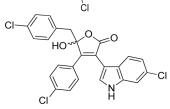	68	7.0±0.2

[a]The experimental error of the measured K_d values is ca. 30%. [b]K_d of compound **2d** could not be determined by NMR.

RESULTS AND DISCUSSION

Design of Novel Antagonists of the Mdm2-p53 Interaction. The patent space of Mdm2 antagonists based on a five-membered heterocyclic core is tightly packed nowadays. Nevertheless, using a three finger pharmacophore model and assuming a five-membered core, we have designed two series of novel compounds, derivatives of 5-hydroxy-1,5-dihydydro-2*H*-pyrrol-2-one and 5-hydroxy-1,5-dihydro-2*H*-furan-2-one. The compounds selected for synthesis and evaluation of their activity are shown in Table 1.

Synthesis of the Substituted 3-Pyrrolin-2-ones. To prepare compounds **1a** and **1b**, we devised a six stage synthetic route (Scheme 1). Compound **5** was easily available from *N*-methylpyrrol (**3**), through the bromination−oxidation procedure[24] (obtaining **4**), and subsequent nucleophilic substitution of a single bromine with 6-chloroindole according to known procedures.[25] Then, a Suzuki−Miyaura reaction allowed substitution of the second bromine with a benzyl moiety resulting in compound **7**.[26] Before that, the N−H proton within 6-chloroindole was protected with *tert*-butyldicarbonate, according to the standard DMAP-catalyzed reaction.[27] The Grignard reaction was used to convert **7** into **8a** and **8b**,[28] and the protecting group was removed under mild conditions by treatment with methylamine solution.[29] Resulting compounds **1a** and **1b** were separated by column chromatography.

Compounds **1c**−**1h** were prepared using a shorter route (Scheme 2). Compound **13** was obtained by cyclization[30] of a (4-chlorophenyl)acetamide (**10**) and a (6-chloro-1*H*-indol-3-yl)oxoacetic acid methyl ester (**12**) previously prepared from commercially available substrates, **9** and **11**, respectively. Compound **13** was methylated to yield monomethylated **14** and dimethylated **15** derivatives or alternatively benzylated to yield **16**. This was done efficiently under mild conditions with potassium carbonate while different evaluated bases (NaH, NaOH, and Cs_2CO_3) led to a number of side-products. Compounds **1c**−**1f** were obtained from **14** and **15**, respectively, using the Grignard reaction as described above for **1a** and **1b**. Compounds **1g**−**1h** were obtained by reduction of **16** with either $NaBH_4$ or alternatively $LiAlH_4$ (ref 31) with similarly high yields. Adapting the shorter synthetic route depicted in Scheme 2 for the preparation of **1a** and **1b** proved impossible due to low yields, multiple side products of the *N*-methylation step, and resulting difficulties in purification.

Synthesis of the Substituted 2-Furanones. Substituted 2-furanones **2a**−**2f** were prepared from a maleimide intermediate of 3-pyrrolin-2-one by trans-cyclization (Scheme 3).[32] Compound **13a** was obtained in the same manner as **13**, from 3-(4-chlorophenyl)propionic amide (**10a**) and (6-chloro-1*H*-indol-3-yl)oxoacetic acid methyl ester (**12**). Substituted maleimides **13** or **13a** were refluxed in basic water−ethanol solution yielding respective substituted maleic anhydrides (**17** and **18**, respectively). These were further modified using the Grignard method as described above to yield substituted 2-furanones **2a**−**2d** and **2e** and **2f**, respectively.

Structure−Activity Relationship. To quantify the affinities of our compounds toward Mdm2, we determined the K_d of

DOI: 10.1021/acschembio.6b00596
ACS Chem. Biol. 2016, 11, 3310−3318

Scheme 1. Synthesis of Compounds 1a and 1b (Numbering of Atoms in the Central Ring of 3-Pyrrolin-2-ones Depicted in Blue)[a]

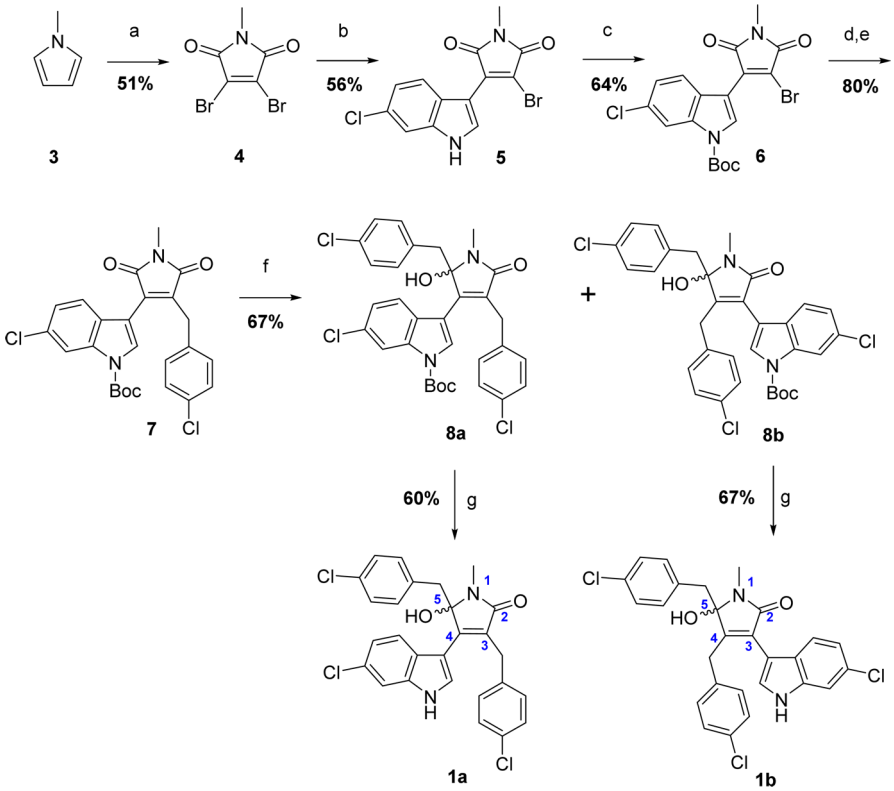

[a]Reagents and conditions: (a) (i) compd **3** (1 equiv), NBS (2.5 equiv), −78 °C to RT, 16 h, anh. THF; (ii) conc. HNO_3, 0 °C, 1 h, hexane. (b) (i) 6-chloroindole (1 equiv), LiHMDS (2.5 equiv), −78 °C, anh. THF; (ii) compd **4** (1 equiv), −20 °C, anh. THF. (c) compd **5** (1 equiv), $(Boc)_2O$ (2 equiv), anh. Et_3N (2 equiv), DMAP (0.1 equiv), RT, 16 h, anh. THF; (d) (i) 4-chlorobenzyl chloride (1.5 equiv), Mg (1.5 equiv), 2 h, reflux, anh. Et_2O; (ii) $B(OMe)_3$ (1 equiv), −78 °C, anh. THF; (iii) KHF_2 (4.5 equiv), H_2O, 0 °C, 0.5 h. (e) compd **6** (1 equiv), potassium (4-chlorobenzyl)trifluoroborate (1.1 equiv), Cs_2CO_3 (3.5 equiv), $Pd(dppf)Cl_2$ complex with CH_2Cl_2 (0.1 equiv), 80 °C, 5 h, toluene/water (5:1). (f) (i) 4-chlorobenzyl bromide (1.5 equiv), Mg (1.5 equiv), 2 h, reflux, anh. Et_2O; (ii) cmpd **7** (1 equiv), 4 h, reflux, anh. THF. (g) compd **8a** or **8b** excess of $MeNH_2$ in MeOH (2 M), 36−72 h, RT.

the compound-Mdm2 interaction using NMR[33,34] and the microscale thermophoresis (MST). For NMR, the ^{15}N-labeled Mdm2 was titrated with increasing concentration of each evaluated compound, and $^{1}H-^{15}N$ 2D-HSQC spectra were recorded after each new portion of the compound was added (Figure 1, Figures S1 and S2).

This method is based on monitoring of chemical shift changes in protein amide backbone resonances upon protein interaction with a small molecule.[34−37] It allows not only qualitative evaluation of the fact of interaction but also to semiquantitative estimation of the binding affinity. Moreover, the strong binding of a small molecule to the target protein, for example, **1d** to Mdm2, results in NMR signal doubling, indicating the K_d's of less than 1 μM (and a slow chemical exchange). Assignment of the amide groups of Mdm2 was obtained after Stoll *et al.*[38] The results are summarized in Table 1.

The compounds substituted with the 4-chlorophenyl group at position 3 of the central ring (**1c−1h**, **2e**, and **2f**, numbering of atoms in the central ring is shown in Schemes 1 and 3) exhibited weak affinity (K_d > 50 μM) regardless of the scaffold being that of 3-pyrrolin-2-one or 2-furanone. At the same time, the compounds substituted at position 3 with the 4-chlorobenzyl group (**1a**, **1b**, **2a−2d**) exhibited better affinities toward Mdm2 compared to the 4-chlorophenyl substituted compounds, again regardless of the core scaffold. It is thus clear that the extra flexibility provided by an additional methylene group is a prerequisite of the efficient binding in these types of compounds. For all tested structural isomers (*i.e.*, **1a** vs **1b** etc.; except **1e** and **1f**), those substituted at position 2 exhibited weaker activities compared to those substituted at position 5, irrespective of the substituent at position 3 and the central ring scaffold. The *N*-methylated 6-chloroindole substituent at position 4 is clearly not compatible with Mdm2 binding as evidenced by weak affinities of compounds **1e** and **1f**.

The affinities of all compounds were additionally tested by microscale thermophoresis (MST; Figure S3). The best binding compounds, **1a** and **2a** demonstrate affinities comparable to those determined by NMR. The occurrence of disparities may be explained by the low solubility of compounds, which was the major issue for NMR. For compounds with NMR K_d's of up to 100 μM, which is considered an "intermediate exchange" NMR range,[35] the MST data demonstrate slightly lower affinities (below 30 μM) compared to NMR data. The apparent NMR K_d's determined in the intermediate exchange range are however expected to be higher than the ones from MST, and the relative differences in affinities of compounds within the series determined using each method are consistent.[39,40] The worst binding compounds (with NMR K_d's higher than 100

DOI: 10.1021/acschembio.6b00596
ACS Chem. Biol. 2016, 11, 3310−3318

Scheme 2. Synthesis of Compounds 1c−1h[a]

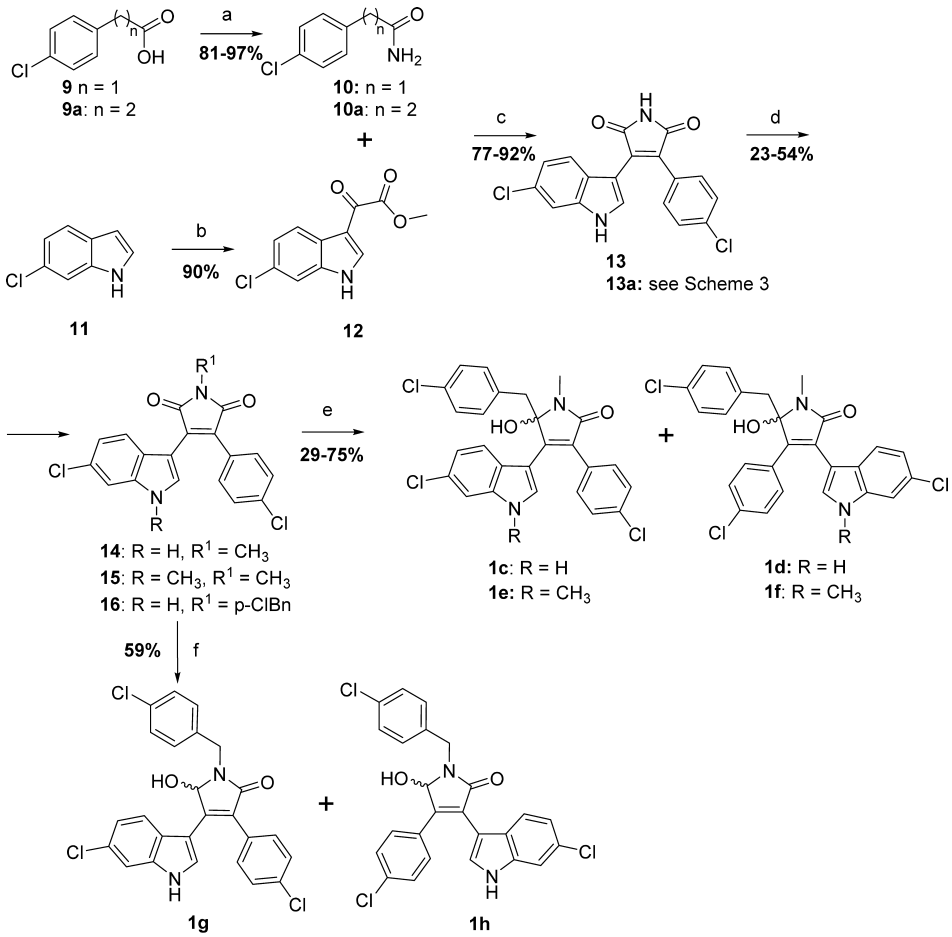

[a]Reagents and conditions: (a) (i) (**9**) or **9a** (1 equiv) thionyl chloride (5 equiv), reflux, 3 h; (ii) $NH_{3(aq)}$ (20 equiv), 0−5 °C to RT, 16 h. (b) (i) 6-chloroindole (**11**) (1 equiv), oxalyl chloride (1.1 equiv), 0 °C, 1 h, anh. THF; (ii) sodium methoxide in MeOH (2 equiv), 60 to 0 °C, 2 h. (c) (i) compd **10** or **10a** (1 equiv), **12** (1 equiv), potassium *tert*-butoxide (4 equiv), 0 °C, 0.5 h, anh. THF; (ii) 55 °C, 5 h; (iii) conc. HCl, RT, 0.5 h. (d) compd **13** (1 equiv), methyl iodide or benzyl bromide (1 equiv), K_2CO_3 (5 equiv), RT, 16 h, anh. DMF. (e) (i) 4-chlorobenzyl bromide (1.5 or 2.5 equiv), Mg (1.5 or 2.5 equiv), 2 h, reflux, anh. Et_2O; (ii) compds **14** or **15** (1 equiv), 4 h, reflux, anh. THF. (f) Compd **16** (1eq), $LiAlH_4$ (2.5 equiv), 0 °C to RT, 1 h, anh. Et_2O-THF.

Scheme 3. Synthesis of Compounds 2a−2f (Numbering of Atoms in the Central Ring of 2-Furanones Depicted in Blue)[a]

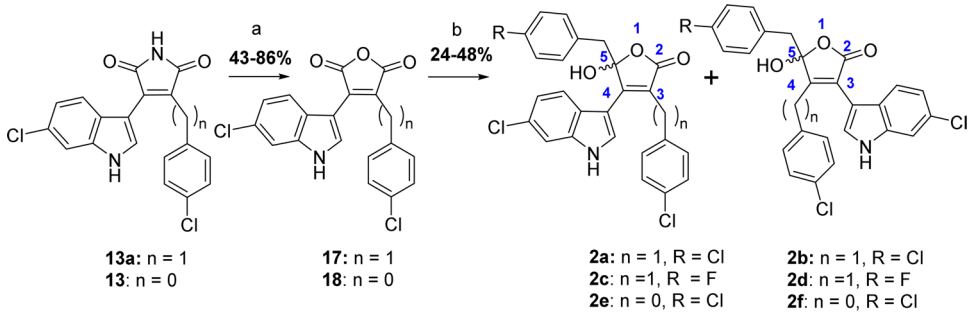

[a]Reagents and conditions: (a) compd **13** or **13a** (1 equiv), NaOH (15 equiv), water/ethanol (5:1), reflux, 1 h. (b) (i) 4-Chlorobenzyl bromide or 4-fluorobenzyl bromide (2.5 equiv), Mg (2.5 equiv), 2 h, reflux, anh. Et_2O; (ii) compds **17** or **18** (1 equiv), 4 h, reflux, anh. THF. The numbering of the central ring is shown in blue based on formulas **2a** and **2b**.

μM) are also characterized by highest values (>30 μM) in MST.

The two "best" identified inhibitors, **1a** and **2a**, show affinities in the low single digit micromolar range. Comparable affinities and the fact that **1a** and **2a** differ only within the central ring scaffold indicate that both scaffolds identified within this study are equally suitable for the further development of Mdm2 inhibitors.

Structural Basis of the Interaction of 1a with Mdm2. In order to better understand the structural basis of interactions of the reported compounds at the binding pocket of Mdm2, we have determined the crystal structure of **1a** in complex with the

DOI: 10.1021/acschembio.6b00596
ACS Chem. Biol. 2016, 11, 3310−3318

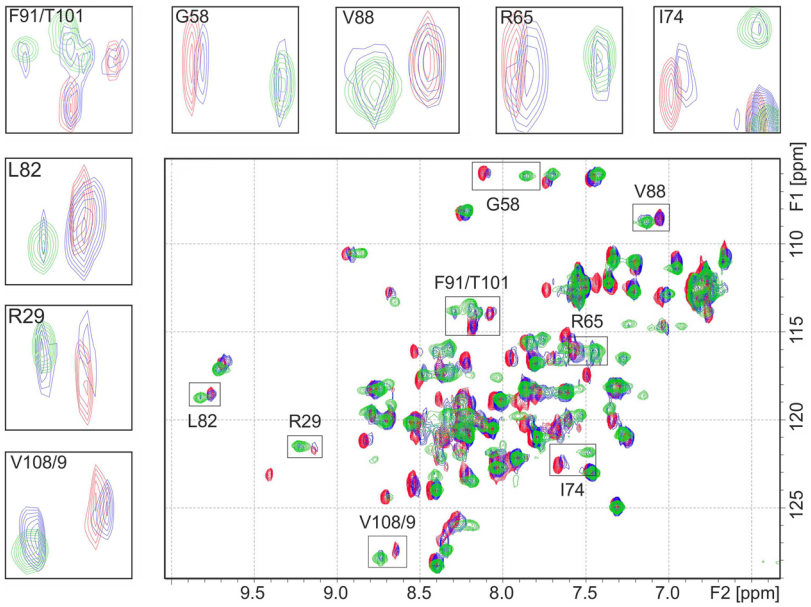

Figure 1. Example NMR spectra for the HSQC-based titration of Mdm2 with **1a**. Red, reference, Mdm2 alone; blue, molar ratio protein/ligand 1:0.5; green, overtitrated Mdm2 (the ratio protein/ligand 1:2).

target protein. The obtained crystals diffracted to 2.0 Å resolution and contain four protein molecules in the asymmetric unit. Each Mdm2 molecule contains a single inhibitor molecule at the binding pocket. No additional inhibitor molecules were found within the structure. The inhibitors were well-defined by their electron density. The Leu26 subpocket is occupied by the 4-chlorobenzyl substituent found at position 3 of **1a**. The aromatic ring of the substituent forms a $\pi-\pi$ stacking interaction with the imidazole ring of His96. The interaction is further stabilized by hydrophobic contacts mediated by the side chains of Leu54, Ile99, and Tyr100. The second 4-chlorobenzyl substituent, located at position 5 of **1a**, occupies the Trp23 subpocket of Mdm2. Its interaction is stabilized by numerous hydrophobic contacts mediated by the side chains of Leu54, Leu57, Ile61, Phe86, Phe91, Ile99, and Ile103 and the C_α of Gly58. The central 3-pyrrolin-2-one ring of the inhibitor molecule covers the entrance to the binding pocket. The oxygen atom of the carbonyl group at position 2 is involved in a water mediated interaction with the N_ε of His96 and the carbonyl oxygen of Val93. The *N*-methyl group forms hydrophobic contact with the side chain of Val93 and is in relatively close contact with the hydroxyl oxygen of Tyr67. Most interestingly, the Phe19 subpocket within Mdm2 is not utilized by the inhibitor. Instead, it is occupied by the side chain of Tyr67, which is oriented differently compared to what is observed in the structure of the Mdm2−p53 complex (Figure 2, Figure S4).

Notably, the 6-chloroindole substituent found at position 4 of **1a** does not occupy the Trp23 pocket as found in a number of structures of previously reported inhibitors. Instead, it interacts with the solvent-exposed residues of Mdm2. The $N_{\varepsilon 1}$ of 6-chloroindole forms a water-mediated interaction with the carbonyl oxygen of Lys51. The significance of this interaction is exemplified by the poor activity of compounds **1e** and **1f**, which are methylated at $N_{\varepsilon 1}$ and, as such, not capable of forming this interaction. Another water molecule, tightly coordinated by the carbonyl oxygen of Phe55 and $N_{\varepsilon 1}$ of Gln59, forms a canonical lone-pair−π interaction with the 6-chloroindole. Finally, the 6-chloroindole forms halogen−π interaction with the aromatic ring of the Phe55 side chain.

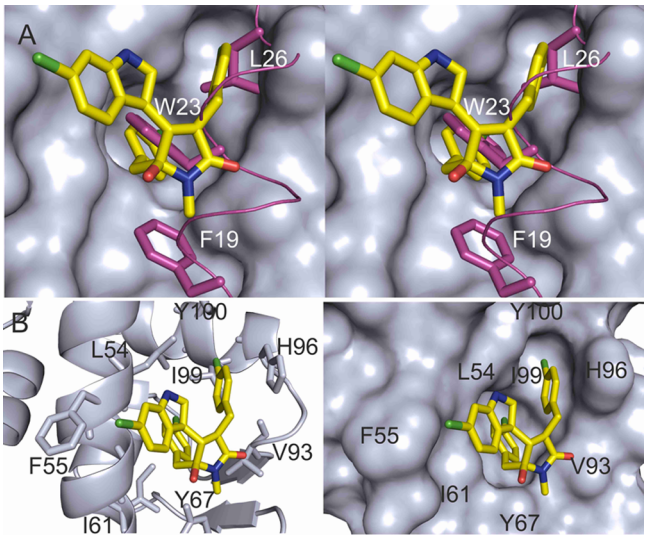

Figure 2. Interaction of the Mdm2 protein and compound **1a** (yellow sticks). (A) Stereoview comparison between the binding modes of **1a** and the p53 peptide (purple; PDB ID: 1YCR).[13] (B) Mdm2−**1a** complex. Left, ribbon representation; right, surface representation.

The Binding Mode of 2a in the p53 Pocket of Mdm2. We also crystallized **2a** in complex with Mdm2 using different crystallization conditions and obtaining crystals exhibiting different arrangement of the molecules within the asymmetric unit compared to the **1a**-containing complex. Despite the differences in overall crystallographic arrangement, the structure of **2a** in complex with Mdm2 demonstrates an almost identical binding mode of **2a** to that observed for **1a**, strongly suggesting that the observed binding mode is compound specific, rather than induced within the crystal. The 4-chlorobenzyl substituents at positions 3 and 5 of **2a** occupy the Leu26 and Trp23 subpockets, respectively, identically as found in the structure containing **1a**. The 2-furanone central

DOI: 10.1021/acschembio.6b00596
ACS Chem. Biol. 2016, 11, 3310−3318

ring is located identically to the 3-pyrrolin-2-one ring of **1a**. The only difference is that the *N*-methyl group is missing in the structure of **2a**, and an additional water mediated interaction between oxygen within the 2-furanone ring and the side chain hydroxyl group of Tyr67 is observed. However, this interaction is present only in one of the molecules contained in the asymmetric unit, which suggests its low contribution to the overall binding energy. This is corroborated by the high temperature factor characterizing the water molecule mediating the interaction. The 6-chloroindole substituent of **2a** is oriented identically to that of **1a** and is involved in analogous interactions. Overall, both compounds **2a** and **1a** and the fragments of Mdm2 containing interacting residues superimpose with an RMSD of 0.21 Å, demonstrating almost identical orientation of both compounds within the Mdm2 binding pocket (Figure 3, Figures S5–S7).

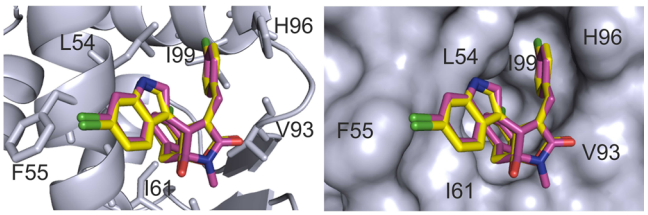

Figure 3. Comparison of the interactions of compounds: **1a** (magenta sticks) and **2a** (yellow sticks) with Mdm2 (shown in ribbon (left panel) and surface (right panel) representation).

Compounds 1a and 2a Induce Dimerization of Mdm2. The arrangement of molecules within the crystal lattice in both structures may suggest the inhibitor-induced dimerization of Mdm2. In the **2a**-containing structure, the asymmetric unit accommodates two Mdm2 molecules which face each other *via* their p53 binding pocket side. This implies that the bound inhibitor molecules also directly face each other. Such a dimer is built around a pseudo-2-fold rotation axis. Mdm2 molecules create multiple hydrogen bonds and water mediated contacts as well as a ring stacking interaction of the Phe55 side chains. The 6-chloroindole moiety of each inhibitor provides a halogen bond[41] with a carbonyl oxygen of Lys51 of the adjacent Mdm2 molecule and water-mediated interaction between the chlorines and $N_{\varepsilon 1}$ atoms of neighboring inhibitor molecules. Identical dimers are recreated by symmetry operations in the **1a**–Mdm2 structure (Figure 4, Figure S8).

To test if the inhibitor induced Mdm2 dimerization observed in the crystal is retained in solution, we recorded ^{1}H NMR spectra of Mdm2 in the presence and absence of **1a**. The addition of **1a** to the Mdm2 containing NMR sample resulted in broadening of the NMR signals of the protein, the NMR line widths being consistent with the induction of the oligomeric state of Mdm2 upon its interaction with **1a** (Figures S9 and S10). This indicates that **1a** induces Mdm2 dimerization in solution, and therefore the dimers observed in the crystal structure reflect biological assemblies and not only crystal packing artifacts.

To further confirm the presence of the dimer in solution, we performed a DOSY NMR experiment. The comparison of log D of the complex of Mdm2 with our compound (**1a**, log D = −9.82) and with RG7388 (ref 42; used as a reference compound which does not induce the dimerization of Mdm2, logD = −9.72) clearly indicates that compound **1a** induces Mdm2 dimerization in solution (Figure S11). This is also

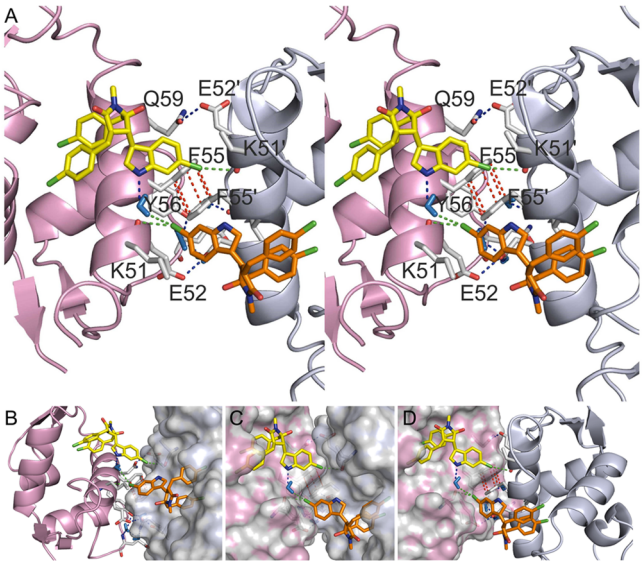

Figure 4. Key interactions that support the dimerization of Mdm2 by **1a**. The Mdm2 molecules forming the dimer: gray and magenta. Residues involved in the Mdm2 dimerization are highlighted as sticks and shown in gray. The inhibitor molecules are shown in yellow and orange. Hydrogen bonds are depicted as blue dotted lines. The ring stacking is depicted as red dotted lines. Halogen bonds are depicted as green dotted lines. Water molecule mediating inhibitor–adjacent Mdm2 molecule interaction is shown in blue. (A) Stereo view. (B–D) Mixed ribbon/surface representations of Mdm2 protein molecules.

confirmed by the hydrodynamic radii calculated from the Stokes–Einstein equation from the DOSY experiments, which were equal to 12.6 and 16.9 Å for the monomer and dimer, respectively.

Discussion and Conclusions. Since the early discovery by García-Echeverría *et al.*[15] that substitution of the indole moiety of Trp23 in the p53 peptide with that of 6-chloroindole significantly potentiates Mdm2 affinity,[15] a large number of small-molecule inhibitors have been developed in which a major interaction with Mdm2 is provided by a 6-chloroindole moiety occupying the Trp23 subpocket. These include, among others, imidazoles,[16] pyrazoles,[43] pyrrolidines,[17] and spiroxindoles.[18] In fact, 6-chloroindole itself binds weakly to Mdm2, as can be appreciated from our NMR titration experiments (Figure S12). The moieties filling the other two subpockets (Phe19 and Leu26) belong to many different classes in previously published inhibitors; however, substituted phenyls and benzyls predominate. Our design approach was initially based on the same premises. Surprisingly, the binding modes of both the 3-pyrrolin-2-one- and 2-furanone-based inhibitors described in this study differ from those anticipated in modeling. In our structures, the 6-chloroindole moiety does not occupy the Trp23 binding pocket but instead provides a number of interactions at the surface of the Mdm2 molecule and with the adjacent Mdm2 and inhibitor molecules thereby inducing dimerization.

Graves *et al.*[44] recently reported a class of Mdm2 inhibitors, exemplified by RO-2443, which induce Mdm2 dimerization by inserting a difluorobenzyl moiety into the Trp23 binding pocket of one Mdm2 molecule and the 6-chloro-7-methylindole moiety into the extended Phe19 pocket of the other Mdm2 molecule within the dimer. The dimeric protein complex is kept together by a dimeric small-molecule core. Therefore, the interaction of RO-2443 with Mdm2 is

DOI: 10.1021/acschembio.6b00596
ACS Chem. Biol. 2016, 11, 3310–3318

comparable to that of the inhibitors described within this study only in the fact that the 6-chloroindole moiety is located outside the Trp23 pocket and that the dimers are stable in solution. The modes by which the inhibitors induce dimerization are, however, completely different, including the fact that the 6-chloroindole moieties of adjacent inhibitors within the dimer do not directly interact in the **1a**- or **2a**-containing structures contrary to that containing RO-2443. Consistently with the different mode of interaction and mechanism of dimerization, the relative orientation of Mdm2 monomers within the dimer is utterly different in the RO-2443-containing structure compared to the **1a**- or **2a**-containing structures (Supporting Text S1, Figure S13).

The SAR for the series of compounds reported in this study is clearly explained by provided crystal structures. The methyl substituent at position 1 of the 3-pyrrolin-2-one ring provides additional hydrophobic contact with Val99 compared to the 2-furanone scaffold, but the absence of a hydrophobic interaction is compensated in the latter scaffold by a weak, water-mediated interaction of the oxygen within the 2-furanone ring and the side chain hydroxyl group of Tyr67. The geometry of the 4-chlorophenyl group at positon 3 of the central ring (**1c**−**1h**, **2e**, and **2f**) is not compatible with the $\pi-\pi$ interaction with the side chain of His96, one of the prominent interactions observed in the structure of **1a** and **2a** containing a more flexible 4-chlorobenzyl at position 3. This explains higher affinities of the 4-chlorobenzyl substituted compounds. Inhibitors substituted at position 5 exhibit higher affinities compared to those substituted at position 2 most probably because the latter are not capable of forming a water mediated interaction of the central ring with the side chain of His96 due to the different orientation of the oxygen atom at position 2. The methyl group at the N_ε atom of the 6-chloroindole substituent prevents its water mediated interaction with the carbonyl oxygen of Lys51, thereby negatively affecting the affinity of such compounds.

Despite the unexpected localization of the 6-chloroindole group in the Mdm2 complexes of the inhibitors described in this study, certain other features describing the inhibitor−Mdm2 interaction are comparable to those previously observed for other Mdm2 inhibitors, rationalizing further optimization of **1a** and **2a** (Supporting Text S2, Figure S14).[45,46] The π-stacking interaction of **1a**/**2a** and His96 of Mdm2 resembles a similar interaction of YH239 (Figure S15B,C).[46] Hydrophobic interactions of chlorobenzyl moieties of **1a** and **2a** at the Leu26 and Trp23 subpockets of the Mdm2 binding site are reminiscent of those of nutlin (Figure S15A) and its derivatives.[47]

In conclusion, we have developed two novel classes of Mdm2 inhibitors. The fact that the inhibitors based on two different scaffolds both interact with Mdm2 in an unexpected, noncanonical fashion opens multiple avenues for further rational optimization.

■ METHODS

Synthesis. Compounds were synthesized as depicted in Schemes 1−3. For details of the reported syntheses and compound analysis, see the Supporting Information.

Protein Expression and Purification. Variants of the N-terminal domain of human Mdm2 were cloned into pET-20 vector (Novagen) and expressed in the *Escherichia coli* BL21(DE3) as described previously.[48] In brief, cells were grown at 37 °C and induced with 1 mM IPTG at an OD_{600} of 0.8 and grown for an additional 5 h at 37 °C. Cells were collected by centrifugation and lysed by sonication. Inclusion bodies were collected by centrifugation, washed with PBS containing 0.05% Triton-X100, and solubilized in 6 M guanidine hydrochloride in 100 mM Tris-HCl at pH 8.0, containing 1 mM EDTA and 10 mM β-mercaptoethanol. The protein was dialyzed against 4 M guanidine hydrochloride at pH 3.5 with 10 mM β-mercaptoethanol. The protein was refolded by dropwise addition into 10 mM Tris-HCl at pH 7.0, containing 1 mM EDTA and 10 mM β-mercaptoethanol and slow mixing overnight at 4 °C. Ammonium sulfate was added to the final concentration of 1.5 M, and the refolded protein was recovered on a Butyl Sepharose 4 Fast Flow (GE Healthcare). The protein was eluted using 100 mM Tris-HCl at pH 7.2, containing 5 mM β-mercaptoethanol and further purified by gel filtration using HiLoad 16/600 Superdex75 (GE Healthcare).

Binding Analysis by Microscale Thermophoresis (MST). MST (NanoTemper Technologies GmbH) was used to determine the binding affinities between Mdm2 (residues 1−118 T47W; 500 nM) and inhibitors. T47W mutation was introduced to facilitate label-free measurements and did not interfere with small molecule binding, as evidenced by unaffected affinity toward a reference compound, nutlin-3. Experiments were performed in 50 mM phosphate buffer at pH 7.4 containing 150 mM NaCl, 5 mM DTT, and 5% DMSO. Inhibitors at increasing concentration (0.763 nM to 25 μM; highest concentration was limited by solubility) were incubated with the protein for 5 min prior to measurement at 25 °C (excitation 280 nm, emission 350 nm). An inhibitor concentration-dependent decrease in tryptophan fluorescence was observed. Inhibitor binding-specific fluorescence quenching was evidenced by a loss of the effect in samples containing the inhibitor, but denatured by heating (95 °C for 5 min) in the presence of 2% SDS and 20 mM DTT. K_d values and uncertainties were calculated using the MO Affinity Analysis software.

NMR Measurements. Uniform ^{15}N isotope labeling was achieved by expression of the protein in the M9 minimal media containing $^{15}NH_4Cl$ as the sole nitrogen source. The final step of purification of Mdm2 (residues 1−118, chosen to enable interactions of N-terminal Mdm2 part[49]) for NMR consisted of gel filtration into the NMR buffer (50 mM phosphate buffer at pH 7.4 containing 150 mM NaCl, 5 mM DTT). Then, 10% (v/v) D_2O was added to the samples to provide a lock signal. All the spectra were recorded at 300 K using a Bruker Avance 600 MHz spectrometer. $^1H-^{15}N$ heteronuclear correlations were obtained using the fast HSQC pulse sequence.[50] Assignment of the amide groups of Mdm2 was obtained after Stoll *et al.*[38]

Crystal Structure Determination. Human Mdm2 (18−125) was prepared in 5 mM Tris−HCl at pH 8.0 containing 50 mM NaCl and 10 mM β-mercaptoethanol. A molar excess (3×) of **1a** or **2a** was added. The Mdm2 inhibitor complex was concentrated to 20 mg mL^{-1}, and screening for crystallization conditions was performed using a sitting drop vapor diffusion method and commercially available buffer sets. Crystals of the Mdm2(18−125)−**1a** complex appeared after a few days at 4 °C in 0.1 M HEPES at pH 7.5 containing 0.2 M sodium chloride and 25% (w/v) PEG 3350. The crystals of the Mdm2(18−111)−**2a** complex were obtained from 0.1 M HEPES at pH 7.5 containing 30% (w/v) PEG 1000. Crystals were flash-cooled in liquid nitrogen without further cryoprotection. The data collection and refinement description and statistics (Table S2) are summarized in the Supporting Information.

The structure factors and final models were deposited into the Protein Data Bank with accession numbers 4ZFI and 4ZGK, for the structure with inhibitors **1a** and **2a**, respectively.

Small-Molecule Crystal Structure Determination. For details of small molecule crystallography experiments, data collection, and compound structures, see the Supporting Information (Figure S16, Table S1).

■ ASSOCIATED CONTENT

Supporting Information

The Supporting Information is available free of charge on the ACS Publications website at DOI: 10.1021/acschembio.6b00596.

DOI: 10.1021/acschembio.6b00596
ACS Chem. Biol. 2016, 11, 3310−3318

Supporting text S1 and S2, synthesis, NMR measurements for K_D determination, crystal structures determination of protein complexes, small-molecule crystal structures determination, supplemental figures and tables, references, and copies of small molecules NMR spectra (PDF)

Accession Codes

The structure factors and final models of Mdm2 complexes with inhibitors were deposited into the Protein Data Bank with the accession numbers 4ZFI and 4ZGK, for the structure containing inhibitors **1a** and **2a**, respectively. All crystallographic data for the small molecule structures have been deposited at the Cambridge Crystallographic Data Centre under accession numbers: CCDC 1054955, **1e**; CCDC 1054956, **1g**; and CCDC 1054957, **1d**.

■ AUTHOR INFORMATION

Corresponding Authors

*E-mail: grzegorz.dubin@uj.edu.pl.
*E-mail: holak@biochem.mpg.de.

Author Contributions

⊥These authors contributed equally to this work.

Notes

The authors declare no competing financial interest.

■ ACKNOWLEDGMENTS

This research has been supported by a Marie Curie FP7-Reintegration-Grants within the seventh European Community Framework Programme, by the project operated within the Foundation for Polish Science TEAM Programme, cofinanced by the EU European Regional Development Fund, and by the Polish National Centre of Science, grant Symphony-2-UMO-2014/12/W/NZ1/00457 (to T.A.H.) and by the Polish National Centre of Science, grant UMO-2011/01/D/NZ1/01169 (to G.D.). A.D. was supported by the National Institutes of Health (1R21GM087617, 1R01GM097082, and 1P41GM094055). E.S. and K.Z. received the scholarship funding for the doctoral thesis preparation from the National Centre of Science, (grants UMO-2014/12/T/ST5/00684 to E.S., UMO-2016/20/T/NZ1/00519 to K.M.Z.). P.G. was supported by the European Union within the SET project and the National Centre of Science (grant UMO-2015/19/D/NZ1/02009). The research was carried out with the equipment purchased thanks to the financial support of the European Union structural funds (contract no. POIG.02.01.00-12-064/08 and POIG.02.01.00-12-167/08) and European Regional Development Fund in the framework of the Polish Innovation Economy Operational Program (contract no. POIG.02.01.00-12-023/08). A.T.-C. has received the financial support from the Faculty of Biochemistry, Biophysics and Biotechnology of Jagiellonian University, which is a partner of the Leading National Research Centre (KNOW) supported by the Ministry of Science and Higher Education. Moreover funding has also been received from the European Union's Horizon 2020 research and innovation programme under MSC ITN "Accelerated Early stage drug dIScovery" (AEGIS), grant agreement No 675555.

■ REFERENCES

(1) Brown, C. J., Lain, S., Verma, C. S., Fersht, A. R., and Lane, D. P. (2009) Awakening guardian angels: drugging the p53 pathway. *Nat. Rev. Cancer 9*, 862−873.

(2) Cheok, C. F., Verma, C. S., Baselga, J., and Lane, D. P. (2011) Translating p53 into the clinic. *Nat. Rev. Clin. Oncol. 8*, 25−37.

(3) Hock, A. K., and Vousden, K. H. (2014) The role of ubiquitin modification in the regulation of p53. *Biochim. Biophys. Acta, Mol. Cell Res. 1843*, 137−149.

(4) Wade, M., Li, Y. C., and Wahl, G. M. (2013) MDM2, MDMX and p53 in oncogenesis and cancer therapy. *Nat. Rev. Cancer 13*, 83−96.

(5) Zhao, Y., Aguilar, A., Bernard, D., and Wang, S. (2015) A potent small-molecule inhibitor of the MDM2-p53 interaction (MI-888) achieved complete and durable tumor regression in mice. *J. Med. Chem. 58*, 1038−1052.

(6) Hoe, K. K., Verma, C. S., and Lane, D. P. (2014) Drugging the p53 pathway: understanding the route to clinical efficacy. *Nat. Rev. Drug Discovery 13*, 217−236.

(7) Vassilev, L. T., Vu, B. T., Graves, B., Carvajal, D., Podlaski, F., Filipovic, Z., Kong, N., Kammlott, U., Lukacs, C., Klein, C., Fotouhi, N., and Liu, E. A. (2004) In vivo activation of the p53 pathway by small-molecule antagonists of MDM2. *Science 303*, 844−848.

(8) Popowicz, G. M., Dömling, A., and Holak, T. A. (2011) The structure-based design of Mdm2/Mdmx-p53 inhibitors gets serious. *Angew. Chem., Int. Ed. 50*, 2680−2688.

(9) Zak, K., Pecak, A., Rys, B., Wladyka, B., Dömling, A., Weber, L., Holak, T. A., and Dubin, G. (2013) Mdm2 and MdmX inhibitors for the treatment of cancer: a patent review (2011-present). *Expert Opin. Ther. Pat. 23*, 425−448.

(10) Uversky, V. N., Dave, V., Iakoucheva, L. M., Malaney, P., Metallo, S. J., Pathak, R. R., and Joerger, A. C. (2014) Pathological unfoldomics of uncontrolled chaos: intrinsically disordered proteins and human diseases. *Chem. Rev. 114*, 6844−6879.

(11) Milroy, L. G., Grossmann, T. N., Hennig, S., Brunsveld, L., and Ottmann, C. (2014) Modulators of protein−protein interactions. *Chem. Rev. 114*, 4695−4748.

(12) Pelay-Gimeno, M., Glas, A., Koch, O., and Grossmann, T. N. (2015) Structure-based design of inhibitors of protein-protein interactions: mimicking peptide binding epitopes. *Angew. Chem., Int. Ed. 54*, 8896−8927.

(13) Kussie, P. H., Gorina, S., Marechal, V., Elenbaas, B., Moreau, J., Levine, A. J., and Pavletich, N. P. (1996) Structure of the MDM2 oncoprotein bound to the p53 tumor suppressor transactivation domain. *Science 274*, 948−953.

(14) Joerger, A. C., and Fersht, A. R. (2008) Structural biology of the tumor suppressor p53. *Annu. Rev. Biochem. 77*, 557−582.

(15) García-Echeverría, C., Chène, P., Blommers, M. J., and Furet, P. (2000) Discovery of potent antagonists of the interaction between human double minute 2 and tumor suppressor p53. *J. Med. Chem. 43*, 3205−3208.

(16) Popowicz, G. M., Czarna, A., Wolf, S., Wang, K., Wang, W., Dömling, A., and Holak, T. A. (2010) Structures of low molecular weight inhibitors bound to MDMX and MDM2 reveal new approaches for p53-MDMX/MDM2 antagonist drug discovery. *Cell Cycle 15*, 1104−1111.

(17) Ding, K. M., Lu, Y., Nikolovska-Coleska, Z., Wang, G., Qiu, S., Shangary, S., Gao, W., Qin, D., Stuckey, J., Krajewski, K., Roller, P. P., and Wang, S. (2006) Structure-based design of potent small-molecule inhibitors of anti-apoptotic Bcl-2 proteins. *J. Med. Chem. 49*, 3432−3435.

(18) Ding, K., Lu, Y., Nikolovska-Coleska, Z., Qiu, S., Ding, Y., Gao, W., Stuckey, J., Krajewski, K., Roller, P. P., Tomita, Y., Parrish, D. A., Deschamps, J. R., and Wang, S. (2005) Structure-based design of potent non-peptide MDM2 inhibitors. *J. Am. Chem. Soc. 127*, 10130−10131.

(19) Michelsen, K., Jordan, J. B., Lewis, J., Long, A. M., Yang, E., Rew, Y., Zhou, J., Yakowec, P., Schnier, P. D., Huang, X., and Poppe, L. (2012) Ordering of the N-terminus of human MDM2 by small molecule inhibitors. *J. Am. Chem. Soc. 134*, 17059−17067.

(20) Bista, M., Wolf, S., Khoury, K., Kowalska, K., Huang, Y., Wrona, E., Arciniega, M., Popowicz, G. M., Holak, T. A., and Dömling, A.

DOI: 10.1021/acschembio.6b00596
ACS Chem. Biol. 2016, 11, 3310−3318

(2013) Transient protein states in designing inhibitors of the MDM2-p53 interaction. *Structure 21*, 2143−2151.
(21) Baek, S., Kutchukian, P. S., Verdine, G. L., Huber, R., Holak, T. A., Lee, K. W., and Popowicz, G. M. (2012) Structure of the stapled p53 peptide bound to Mdm2. *J. Am. Chem. Soc. 134*, 103−106.
(22) Chang, Y. S., Graves, B., Guerlavais, V., Tovar, C., Packman, K., To, K. H., Olson, K. A., Kesavan, K., Gangurde, P., Mukherjee, A., Baker, T., Darlak, K., Elkin, C., Filipovic, Z., Qureshi, F. Z., Cai, H., Berry, P., Feyfant, E., Shi, X. E., Horstick, J., Annis, D. A., Manning, A. M., Fotouhi, N., Nash, H., Vassilev, L. T., and Sawyer, T. K. (2013) Stapled α-helical peptide drug development: a potent dual inhibitor of MDM2 and MDMX for p53-dependent cancer therapy. *Proc. Natl. Acad. Sci. U. S. A. 110*, E3445−E3454.
(23) Vogel, S. M., Bauer, M. R., Joerger, A. C., Wilcken, R., Brandt, T., Veprintsev, D. B., Rutherford, T. J., Fersht, A. R., and Boeckler, F. M. (2012) Lithocholic acid is an endogenous inhibitor of MDM4 and MDM2. *Proc. Natl. Acad. Sci. U. S. A. 109*, 16906−16910.
(24) Choi, D. S., Huang, S., Huang, M., Barnard, T. S., Adams, R. D., Seminario, J. M., and Tour, J. M. (1998) Revised structures of N-substituted dibrominated pyrrole derivatives and their polymeric products. Termaleimide models with low optical band gaps. *J. Org. Chem. 63*, 2646−2655.
(25) Bourderioux, A., Routier, S., Bénéteau, V., and Mérour, J. Y. (2007) Synthesis of benzo analogs of oxoarcyriaflavins and caulersine. *Tetrahedron 63*, 9465−9475.
(26) Molander, G. A., Ham, J., and Seapy (2007) D. G. Palladium-catalyzed cross-coupling reaction of alkenyl bromides with potassium alkyltrifluoroborates. *Tetrahedron 63*, 768−775.
(27) Wang, K., and Liu, Z.-Z. (2010) Synthesis of *N*-methyl-bisindolylmaleimide amino acid methyl ester conjugates and cytotoxicity study. *Eur. J. Med. Chem. 45*, 4175−4179.
(28) Watson, A. F., Liu, J., Bennaceur, K., Drummond, C. J., Endicott, J. A., Golding, B. T., Griffin, R. J., Haggerty, K., Lu, X., McDonnell, J. M., Newell, D. R., Noble, M. E. M., Revill, C. H., Riedinger, C., Xu, Q., Zhao, Y., Lunec, J., and Hardcastle, I. R. (2011) MDM2-p53 protein−protein interaction inhibitors: A-ring substituted isoindolinones. *Bioorg. Med. Chem. Lett. 21*, 5916−5919.
(29) Ohkubo, M., Nishimura, T., Jona, H., Honma, T., and Morishima, H. (1996) Practical synthesis of indolopyrrolocarbazoles. *Tetrahedron 52*, 8099−8112.
(30) Faul, M. M., Winneroski, L. L., and Krumrich, C. A. (1998) A new, efficient method for the synthesis of bisindolylmaleimides. *J. Org. Chem. 63*, 6053−6058.
(31) Mahboobi, S., Dove, S., Kuhr, S., and Pongratz, H. (1999) Synthesis of arcyriarubine regioisomersi by Pd(0) catalysis or via lithiated indol derivatives − conformational analysis by semiempirical and X-ray methods. *Pharmazie 54*, 820−827.
(32) Davis, P. D., Hill, C. H., Lawton, G., Nixon, J. S., Wilkinson, S. E., Hurst, S. A., Keech, E., and Turner, S. E. (1992) Inhibitors of protein kinase C. 1. 2,3-bisarylmaleimides. *J. Med. Chem. 35*, 177−184.
(33) Markin, C. J., and Spyracopoulos, L. (2012) Increased precision for analysis of protein−ligand dissociation constants determined from chemical shift titrations. *J. Biomol. NMR 53*, 125−138.
(34) Powers, R. (2009) Advances in nuclear magnetic resonance for drug discovery. *Expert Opin. Drug Discovery 4*, 1077−1098.
(35) Shuker, S. B., Hajduk, P. J., Meadows, R. P., and Fesik, S. W. (1996) Discovering high-affinity ligands for proteins: SAR by NMR. *Science 274*, 1531−1534.
(36) Barile, E., and Pellecchia, M. (2014) NMR-based approaches for the identification and optimization of inhibitors of protein−protein interactions. *Chem. Rev. 114*, 4749−4763.
(37) Skinner, A. L., and Laurence, J. S. (2008) High-field solution NMR spectroscopy as a tool for assessing protein interactions with small molecule ligands. *J. Pharm. Sci. 97*, 4670−4695.
(38) Stoll, R., Renner, C., Hansen, S., Palme, S., Klein, C., Belling, A., Zeslawski, W., Kamionka, M., Rehm, T., Muhlhahn, P., Schumacher, R., Hesse, F., Kaluza, B., Voelter, W., Engh, R. A., and Holak, T. A. (2001) Chalcone derivatives antagonize interactions between the human oncoprotein MDM2 and p53. *Biochemistry 40*, 336−344.
(39) Wüthrich, K. (1986) *NMR of Proteins and Nucleic Acids*, Viley-VCH, Weinheim, Germany, ISBN: 978-0-471-82893-8.
(40) Meyer, B., and Peters, T. (2003) NMR spectroscopy techniques for screening and identifying ligand binding to protein receptors. *Angew. Chem., Int. Ed. 42*, 864−890.
(41) Wilcken, R., Zimmermann, M. O., Lange, A., Joerger, A. C., and Boeckler, F. M. (2013) Principles and applications of halogen bonding in medicinal chemistry and chemical biology. *J. Med. Chem. 56*, 1363−1388.
(42) Ding, Q., Zhang, Z., Liu, J.-J., Jiang, N., Zhang, J., Ross, T. M., Chu, X.-J., Bartkovitz, D., Podlaski, F., Janson, C., Tovar, C., Filipovic, Z. M., Higgins, B., Glenn, K., Vassilev, L. T., Graves, D., and Packman, K. (2013) Discovery of RG7388, a potent and selective p53−MDM2 inhibitor in clinical development. *J. Med. Chem. 56*, 5979−5983.
(43) Dömling, A., and Holak, T. A. (2012) Novel p53-mdm2/p53-mdm4 antagonists to treat proliferative disease. Patent WO2011106650.
(44) Graves, B., Thompson, T., Xia, M., Janson, C., Lukacs, C., Deo, D., Di Lello, P., Fry, D., Garvie, C., Huang, K. S., Gao, L., Tovar, C., Lovey, A., Wanner, J., and Vassilev, L. T. (2012) Activation of the p53 pathway by small-molecule-induced MDM2 and MDMX dimerization. *Proc. Natl. Acad. Sci. U. S. A. 109*, 11788−11793.
(45) Huang, Y., Wolf, S., Beck, B., Köhler, L. M., Khoury, K., Popowicz, G. M., Goda, M., Subklewe, S. K., Twarda, A., Holak, T. A., and Dömling, A. (2014) Discovery of highly potent p53-MDM2 antagonists and structural basis for anti-acute myeloid leukemia activities. *ACS Chem. Biol. 9*, 802−811.
(46) Grace, C. R., Ban, D., Min, J., Mayasundari, A., Min, L., Finch, K. E., Griffiths, L., Bharatham, N., Bashford, D., Kiplin Guy, R., Dyer, M. A., and Kriwacki, R. W. (2016) Monitoring ligand-induced protein ordering in drug discovery. *J. Mol. Biol. 428*, 1290−1303.
(47) Anil, B., Riedinger, C., Endicott, J. A., and Noble, M. E. (2013) The structure of an MDM2-Nutlin-3a complex solved by the use of a validated MDM2 surface-entropy reduction mutant. *Acta Crystallogr., Sect. D: Biol. Crystallogr. 69*, 1358−1366.
(48) Czarna, A., Popowicz, G. M., Pecak, A., Wolf, S., Dubin, G., and Holak, T. A. (2009) High affinity interaction of the p53 peptide-analogue with human Mdm2 and Mdmx. *Cell Cycle 8*, 1176−1184.
(49) Showalter, S. A., Bruschweiler-Li, L., Johnson, E., Zhang, F., and Brüschweiler, R. (2008) Quantitative Lid Dynamics of MDM2 Reveals Differential Ligand Binding Modes of the p53-Binding Cleft. *J. Am. Chem. Soc. 130*, 6472−6478.
(50) Mori, S., Abeygunawardana, C., Johnson, M. O., and van Zijl, P. C. (1995) Improved sensitivity of HSQC spectra of exchanging protons at short interscan delays using a new fast HSQC (FHSQC) detection scheme that avoids water saturation. *J. Magn. Reson., Ser. B 108*, 94−98.

DOI: 10.1021/acschembio.6b00596
ACS Chem. Biol. 2016, 11, 3310−3318